Pakistan Veterinary Journal

ISSN: 0253-8318 (PRINT), 2074-7764 (ONLINE)
DOI: 10.29261/pakvetj/2026.043

RESEARCH ARTICLE

Polystyrene Nanoplastics Exacerbate CCl_4-Induced Liver Fibrosis by Aggravating Stretch-Induced Mechanical Stress in Hepatic Stellate Cells

Jae-Hyuk Yim[1], Tae-Un Kim[1], Woo Jun Kim[1], Hee-Yeon Kim[3], Seoung-Woo Lee[3], Kyung-Ku Kang[4], Min-Soo Seo[5], Sung Dae Kim[5], Young-Eun Cho[6], Su-Min Baek[1], Seong-Kyoon Choi[3] and Jin-Kyu Park[1, 2, *]

[1]Department of Veterinary Pathology, College of Veterinary Medicine, Kyungpook National University, Daegu 41566, Republic of Korea; [2]Institute for Veterinary Biomedical Science, Kyungpook National University, Daegu 41566, Republic of Korea; [3]Core Protein Resources Center, Daegu-Gyeongbuk Institute of Science and Technology (DGIST), Daegu 42988, Republic of Korea; [4]Preclinical Research Center, Daegu-Gyeongbuk Medical Innovation Foundation, Daegu 41016, Republic of Korea; [5]College of Veterinary Medicine, Kyungpook National University, Daegu 41566, Republic of Korea; [6]Department of Food Science and Nutrition, Andong National University, Andong 36729, Republic of Korea
*Corresponding author: jinkyu820@knu.ac.kr

ARTICLE HISTORY (25-1032)

Received: October 25, 2025
Revised: March 09, 2026
Accepted: March 10, 2026
Published online: March 11, 2026

Key words:
Polystyrene nanoplastic
Liver fibrosis
HSC activation
Smad2/3
Mechanical stress

ABSTRACT

Although studies on the potential hepatotoxicity of nanoplastic depositions are being conducted, there remains a lack of research on the association between nanoplastic depositions and chronic liver disease. Therefore, this research aimed to explore the influence of polystyrene nanoparticles (PS-NPs) on the progression of liver fibrosis and the mechanisms involved in the hepatic stellate cells (HSCs) activation. Chronic exposure to PS-NPs aggravated CCl_4-induced liver fibrosis, as evidenced by enhanced collagen accumulation and elevated α-smooth muscle actin (α-SMA) expression. Most PS-NPs were accumulated in non-parenchymal liver cells, with Kupffer cells exhibiting the highest uptake. This accumulation was associated with enhanced recruitment of CD68-positive macrophages. However, PS-NPs were not associated with TGF-β expression in CD68-positive cells. Additionally, CD68-positive cells treated with PS-NPs did not affect α-SMA expression in HSCs. Further in vitro experiments revealed that α-SMA and pSmad2/3 were directly promoted by PS-NPs in both LX-2 HSCs and primary isolated HSCs, indicating a direct stimulatory effect on HSC activation. PS-NPs enhanced pTGFBR1 expression of HSCs by promoting stretch-induced mechanical stress, suggesting a novel pathway through which nanoplastics may exacerbate fibrogenesis. Our findings provide the first evidence that PS-NPs, as xenobiotic particles, can directly promote HSC activation and exacerbate liver fibrosis, indicating potential health risks associated with chronic nanoplastic exposure.

To Cite This Article: Yim JH, Kim TU, Kim WJ, Kim HY, Lee SW, Kang KK, Seo MS, Kim SD, Cho YE, Baek SM, Choi SK and Park JK, 2026. Polystyrene nanoplastics exacerbate CCl_4-induced liver fibrosis by aggravating stretch-induced mechanical stress in hepatic stellate cells. Pak Vet J, 46(3): 544-555. http://dx.doi.org/10.29261/pakvetj/2026.043

INTRODUCTION

Global plastic pollution is steadily increasing due to the increasing production and use of plastics (Savoca *et al.,* 2016). Indeed, commonly utilized plastics, such as polystyrene, polypropylene, and polyethylene, are being gradually decomposed in the environment and are easily fragmented by environmental forces. Polystyrene is a thermoplastic that softens on heating and hardens on cooling; thus, polystyrene plastics represent the most abundant small-sized plastics found in the environment (Barnes *et al.,* 2009; Gupta *et al.,* 2022). Gradual breakdown of larger plastics made small-sized plastic *wastes*, ultimately forming microplastics (<5000μm) or nanoplastics (<1μm) (Hale *et al.,* 2020). Microplastics and nanoplastics can be accumulated in the bodies of aquatic organisms, mice and humans (Deng *et al.,* 2017; Lee *et al.,* 2019; Oliveri *et al.,* 2020; Şimsek *et al.,* 2025). Furthermore, small-sized plastics are easily absorbed into the circulatory system of living organisms (Nor *et al.,* 2021; Sharma *et al.,* 2023). According to the previous study, nanoplastics were found in several organs and induce inflammation and cytotoxicity (Kwon *et al.,* 2022). Specifically, nanoplastics predominantly accumulate in the liver (Khan and Jia, 2023). A previous study demonstrated that microplastic accumulation in the liver was facilitated

by ethanol ingestion and accelerated lipid accumulation (Baek *et al.,* 2023). While liver damage caused by nanoplastics has been noted, there is a lack of research on the mechanisms through which polystyrene nanoparticles (PS-NPs) stimulate chronic liver diseases (Chen *et al.,* 2025).

Liver fibrosis, a reversible chronic liver disease, is caused by a dysregulated wound-healing process driven by activated hepatic stellate cells (HSCs) (Wells, 2005; Ding *et al.,* 2021; Xu *et al.,* 2021). HSCs typically remain in a quiescent state, supporting the space of Disse. However, these cells become activated into myofibroblasts through various mechanisms, including oxidative stress, cholesterol metabolism, liver sinusoidal endothelial cell (LSEC) capillarization, and mechanical stress (Tsuchida and Friedman, 2017; Yanguas *et al.,* 2016; Yi *et al.,* 2015). These activated HSCs produce an extracellular matrix (ECM), which promotes liver fibrosis. Meanwhile, transforming growth factor-beta (TGF-β) is a key cytokine for HSC activation, which binds to TGF-β receptor 2 (TGFBR2) and facilitates the phosphorylation of TGF-β receptor 1 (TGFBR1) (Gupta *et al.,* 2019). The phosphorylated TGFBR1 (pTGFBR1) recruits and phosphorylates Smad2/3, which then acts as a transcription factor regulating various fibrogenic protein expressions (Xu *et al.,* 2015; Cheng *et al.,* 2025). However, the underlying mechanisms and mediators associated with HSC activation have yet to be elucidated. Furthermore, the mechanisms and effects of nanoplastics on liver fibrosis are still unclear.

Some studies have shown that PS-NPs produce reactive oxygen species (ROS), which induce cellular damage and inflammatory responses, thereby exacerbating liver injury (Hu and Palic, 2020). PS-NPs induce hepatocellular apoptosis, inflammatory infiltration, and disrupt normal liver metabolic functions (Yasin *et al.,* 2022). These pathological alterations activate HSCs, which is crucial for the development of liver fibrosis. Therefore, this study examined the influence of chronic PS-NP accumulation on liver fibrosis development and the mechanisms driving HSC activation.

MATERIALS AND METHODS

Animals and experimental design: The Kyungpook National University's IACUC approved all animal experiments (Approval no. 2022-0412). All animal experimental procedures and care were performed in accordance with the ARRIVE guidelines. Under specific pathogen-free facility, all mice were housed at 22-24℃, a 12-hour light/dark cycle, and 40-50% humidity, providing unrestricted water and standard chow. At the end of the experimental period, the mice were humanely euthanized using 240 mg/kg of 1.2% Avertin® (T48402; Sigma-Aldrich, MO, USA) to minimize animal suffering. Six groups were formed from ten-week-old C57BL/6 male mice (n = 28): vehicle (n=5), PS-NP (n=5), 3-week CCl_4 (n=4), 3-week CCl_4 + PS-NP (n=4), 12-week CCl_4 (n=5), and 12-week CCl_4+PS-NP (n=5). The PS-NP groups received intraperitoneal injections of 200 nm fluorescent PS-NPs (FP-0252-2, Spherotech, IL, USA) at concentration of 0.5mg/kg, five times a week. According to previous study, the maximum concentration of PS plastic particles detected in human blood is 4.8 μg/mL (Leslie *et al.,* 2022). Based on a standard mouse blood volume of 72mL/kg, the average concentration of PS-NPs in mouse blood is approximately 0.346mg/kg (Poitout-Belissent *et al.,* 2016). To efficiently deliver PS-NPs to the liver, intraperitoneal administration was selected. Considering the reported bioavailability of 70–78% for IP administration a dosage of 0.5 mg/kg of PS-NPs was selected (Lin *et al.,* 2015). The CCl_4 groups were treated with CCl_4 (2.5mL/kg in 10% olive oil) three times a week. This dosage was adopted and modified from well-established murine hepatic fibrosis models (Park *et al.,* 2009; Lin *et al.,* 2017; Sun *et al.,* 2018). The groups receiving treatment for 3 weeks were sacrificed at week 3, while those in the other groups were sacrificed at week 12, following the first treatment. After necropsy and blood collection, liver samples were rapidly fixed in 10% formalin and 4% paraformaldehyde or flash-frozen.

Histopathological analysis: For hematoxylin and eosin (H&E) stain, paraffin-embedded liver sections were stained and mounted using Canada balsam. All histopathological grades were processed from at least five fields at 200X magnification, following the modified Nonalcoholic Steatohepatitis Clinical Research Network criteria and Metavir fibrosis grading system (Kleiner *et al.,* 2005; Faria *et al.,* 2009).

Masson's trichrome staining: Masson's trichrome staining was performed following previously described method (Jung *et al.,* 2024; Kim *et al.,* 2025). Deparaffinized tissue sections were stained with Weigert's iron hematoxylin for 10min and were rinsed with warm tap water and stained in Biebrich scarlet-acid fuchsin solution for 15min. Differentiation steps included phosphomolybdic-phosphotungstic acid for 15min, aniline blue for 5-10min, and a brief 1% acetic acid wash. Stained sections were dehydrated, cleared in toluene, and mounted.

Hydroxyproline assay: The hydroxyproline (HYP) content was quantified using a modified version of a previously described method (Tashiro *et al.,* 2013). A 50mg frozen liver tissues were homogenized in 500μL of DW, mixed with 500μL 12N HCl, then heated at 120°C, 3h. After cooling, the samples were filtered through filter paper (1004-110, Whatman, Kent, UK). Then, 10μL homogenate or standard HYP solutions were evaporated to dryness at 65°C. After chloramine-T solution adding, samples were incubated at room temperature (RT), 20min and followed by perchloric acid for 5min. Then, dimethyl benzaldehyde solution in methoxyethanol was added and incubated at 60°C, 25min. After cooling, 560nm absorbance was measured by BioTek Epoch 2 Microplate Spectrophotometer (BioTek, VT, USA)

Immunofluorescence staining and confocal microscopy: 4μm cryosections were blocked with 5% donkey serum at RT, 1h. The slides were incubated with rat anti-CD68 (MCA 1957GA, Bio-Rad, CA, USA), rabbit anti-α-SMA (ab124964, Abcam, MA, USA), rabbit anti-Smad2/3 (sc8332, Santa Cruz Biotechnology, TX, USA), rabbit anti-pSmad2/3 (#8828, Cell Signaling Technology, MA, USA), rabbit anti-pTGFBR1 (CSB-PA050248,

Cusabio, TX, USA) at 4°C overnight. After rinsing, incubation at RT in the dark for 1h with donkey anti-rabbit-555 IgG (ab150066, Abcam) and donkey anti-rat-555 IgG (ab150154, Abcam) was performed. Finally, prolonged DAPI (8961S, Cell Signaling Technology) used for mounting the sides. The ratio of the α-SMA area and the number of CD68-positive cells and PS-NPs was measured by ImageJ (National Institutes of Health, MD, USA) from five random fields at 200X magnification. Confocal microscopy was conducted using a Carl Zeiss LSM800 super-resolution confocal laser-scanning microscope. Image acquisition and analysis were performed using ZEN 2.3 Lite.

Western blot analysis: Liver tissue and cell proteins were extracted by 1x sample buffer diluted in VJ lysis buffer. This solution was activated by sodium pyrophosphate, sodium fluoride, 0.1mM sodium vanadate, Pefabloc SC (Roche Diagnostics, Basel, Switzerland), and protease inhibitors (Roche Diagnostics). A 10% SDS-PAGE gel was used for loading protein samples, which were subsequently transferred to Immobilion-P (EMD Millipore Corporation, MA, USA). After rinsing with 1x TBS, then the membranes were blocked at RT for 1h with 5% skim milk or 5% BSA in 1x TBS containing Tween 20 (TBS/T). The membranes were briefly rinsed with 1x TBS and then incubated overnight at 4°C with the primary antibody. After TBS/T wash, goat-anti-rabbit (401393, Calbiochem, CA, USA) was applied to the membranes for secondary antibody at RT, 1h. Then, ECL (TransLab) solution was used for membrane development, and Fusion Solo S (Vilber Lourmat, Eberhardzell, Germany) was used for visualization. Following antibodies were used: rabbit anti-α-SMA (ab124964, Abcam), rabbit anti-pSmad2/3 (#8828, Cell Signaling Technology), rabbit anti-SMAD2/3 (sc8332, Santa Cruz Biotechnology), rabbit anti-TGFBR1 (AF5347, Affinity Biosciences, OH, USA), rabbit anti-pTGFBR1 (CSB-PA050248, Cusabio). As an internal standard, rabbit anti-GAPDH (#2118, Cell Signaling Technology) was used.

Quantitative reverse transcription-polymerase chain reaction (qRT-PCR): Using TRIzol solution (TS200-001, BioScience Technology, Daegu, Republic of Korea), RNA was extracted from snap-frozen liver tissues and cells. RNA concentration was measured with a ND-1000 spectrophotometer (NanoDrop Technologies, DE, USA). The RT Prime kit (EBT-1520, ELPIS Biotech, Daejeon, Republic of Korea) was utilized for cDNA synthesis. After primer and SYBR Green (RT500M; Enzynomics, Daejeon, Korea) were mixed with cDNA samples, qRT-PCR was performed. For the loading control, 18S ribosomal RNA was used to normalize gene expression.

Cell culture and in vitro experiment: The LX-2 cell line was generously provided by Prof. Young-Eun Cho, Department of Food and Nutrition, Andong National University, Andong, South Korea. LX-2 cells were cultured in DMEM (WelGENE Inc., Gyengsan, Republic of Korea) containing 10% FBS (Gibco, CA, USA) and 1% antibiotics (WelGENE Inc.). After seeding on 12-well plates for 1×10^5 cells, 200 μg/mL dyed (FP-0252-2) or non-dyed (PP-015-10) PS-NPs diluted in serum-free DMEM were treated on LX-2 cells for 24h. The cells were harvested and used for immunofluorescence and Western blot analyses.

RAW 264.7 cells were cultured in DMEM containing 10% FBS and 1% antibiotics. For PS-NP treatment, 1×10^5 cells were seeded on 12-well plates and treated with 200μg/mL PS-NPs for 24h. The cells were harvested for qRT-PCR and cell supernatants were collected for LX-2 cell co-culture.

Measurement of TGF-β1 levels by ELISA: The total amount of TGF-β1 was analyzed using ELISA kits (DY1679-05, R&D Systems Inc., MN, USA) according to the manufacturer's protocol. As the final visualization substrate, 1-Step Slow TMB-ELISA (Thermo, MA, USA) was used, and a stop solution (2M H_2SO_4) was added. The solution in the well was detected at 450nm wavelength using an Epoch2 microplate reader (Bio-Tek Instruments, VT, USA).

Primary non-parenchymal cells isolation: Cells were isolated from C57BL/6 mouse livers using 1X EGTA buffer and collagenase type 2 (LS004176; Worthington Biochemical Corporation, Lakewood, NJ) for liver perfusion and digestion. Filtered cells were centrifuged at 500rpm, 5min to ensure separation from hepatocytes. The remaining supernatants were centrifuged at 2000rpm, 4°C, 10min to collect non-parenchymal cells (NPCs). Then, the NPCs were plated into 12-well plates or onto coverslips with 10% FBS containing RPMI 1640 media for 24h and harvested for FACS analysis.

Primary HSC isolation: For primary HSCs isolation, the NPC pellets were suspended in HBSS (LB003-01; WelGENE Inc.) and subsequently centrifuged at 1600rpm for 10min, 4°C. The NPC fraction was resuspended in 15% OptiPrep (D1556; Sigma-Aldrich, MO, USA), added with 11.5% OptiPrep at the upper layer of the cell suspension, as well as with HBSS at the top layer. After centrifugation at 3000rpm, 4°C, 17min, the HSCs fraction was obtained at the interface of the intermediate and top layers. The primary HSCs were cultured in 10% FBS containing DMEM with 1% antibiotics, and 1% L-glutamine. After incubating, the HSCs were treated with or without 200μg/mL PS-NPs and 10μM SB525334 (HY-12043, MedChemExpress, NJ, USA). The cells were washed and harvested at 6 h or 24 h after treatment for Western blot analysis.

Flow cytometry of isolated NPCs: For isolated NPCs staining, rat anti-CD68, rabbit anti-endothelial nitric oxide synthase (eNOS; NB300-500, Novus Biological, Cambridge, UK), mouse anti-desmin (sc-23879, Santa Cruz Biotechnology), rabbit anti-α-SMA (ab124964, Abcam), or mouse anti-α-SMA (A2547, Sigma) were used. The cells were fixed with 4% paraformaldehyde and then permeabilized with 0.1% Triton X-100. Following washing, donkey anti-mouse or rabbit-488 IgG, donkey anti-mouse or rabbit or rat-647 IgG (Abcam) were treated at RT, 30 min. BD Accuri™ C6 Plus flow cytometer (BD FACS, CA, USA) and following software were used for flow cytometry.

Statistical analysis: All data values are shown as the mean±standard deviation. Significance was determined by unpaired Student's t-test or one-way analysis with post hoc testing, with P-value of less than 0.05 considered significant.

RESULTS

PS-NPs aggravated CCl_4-induced liver fibrosis and enhanced α-SMA expression: For 12 weeks, PS-NPs or CCl_4 were administered intraperitoneally five times a week (Fig. 1A). To enable visualization, the PS-NPs were labeled with fluorescent dye and subsequently examined under a fluorescent microscope (Fig. 1B). In histological analysis, PS-NP tended to induce more severe ballooning degeneration and inflammatory cell infiltration, particularly in 3-week CCl_4+PS-NP group (Fig. 1C-E).

In MT staining, the grade of CCl_4-induced liver fibrosis was increased by PS-NPs, and this was prominently confirmed at 12-week CCl_4+PS-NP group (Fig. 2A, B). Furthermore, the 12-week CCl_4+PS-NP group showed a tendency toward higher HYP levels compared with the 12-week CCl_4 group (Fig. 2C). In the immunohistochemistry (IHC) staining analysis, the α-SMA-positive area was significantly increased in the PS-NP administered groups (Fig. 2D, E). Similarly, an increase in α-SMA expression was noted following PS-NP administration, with the exception of the 12-week CCl_4+PS-NP group (Fig. 2F, G). These results suggest that PS-NPs aggravated CCl_4-induced hepatic injury and were associated with increased collagen deposition in advanced stages. The exception observed in the 12-week CCl_4+PS-NP group suggests that the robust liver injury induced by 12 weeks of CCl_4 administration masked the damage caused by PS-NPs.

PS-NPs predominantly accumulated in non-parenchymal cells: To confirm whether PS-NPs accumulate in the liver, fluorescence microscope were used (Fig. 3A). More PS-NPs were detected in 12-week CCl_4+PS-NP livers than in PS-NP group livers and 3-week CCl_4+PS-NP livers (Fig. 3B). Additionally, the PS-NPs were rarely found in hepatocytes; as liver fibrosis progressed, the proportion found in hepatocytes further decreased (Fig. 3C). Thus, it was expected that PS-NPs would mainly accumulate in NPCs and primarily affect NPCs. Therefore, FACS analysis was performed on isolated NPCs treated with fluorescently dyed PS-NPs to confirm which NPCs most actively engulfed PS-NPs (Fig. 3D, E). Notably, PS-NPs were most abundant in Kupffer cells (KCs), followed by LSECs and HSCs (Fig. 3F–I).

PS-NPs were most highly engulfed by Kupffer cells and induced the recruitment of CD68-positive cells: Since KCs mainly engulfed PS-NPs, CD68 expression patterns were then examined to assess the relationship between PS-NP accumulation and KCs (Fig. 4A). Immunofluorescent (IF) staining for CD68 revealed that co-administration of CCl_4 and PS-NPs increased CD68-positive cells compared with only the CCl_4-treated groups; however, there was no difference in the vehicle groups (Fig. 4B). As the number of PS-NPs increased, the number of CD68-positive cells that engulfed PS-NPs also increased (Fig. 4C). Additionally, many CD68-positive cells co-localized with PS-NPs (Fig. 4D). To confirm the response of KCs on PS-NPs, the expression levels of TGF-β in liver tissue were evaluated. Consistent with the CD68-positive cell counts, co-administration of CCl_4 and PS-NPs elevated *TGF-β* gene expression in liver tissue compared with the CCl_4-treated groups alone; however, no difference was observed in the vehicle groups (Fig. 4E).

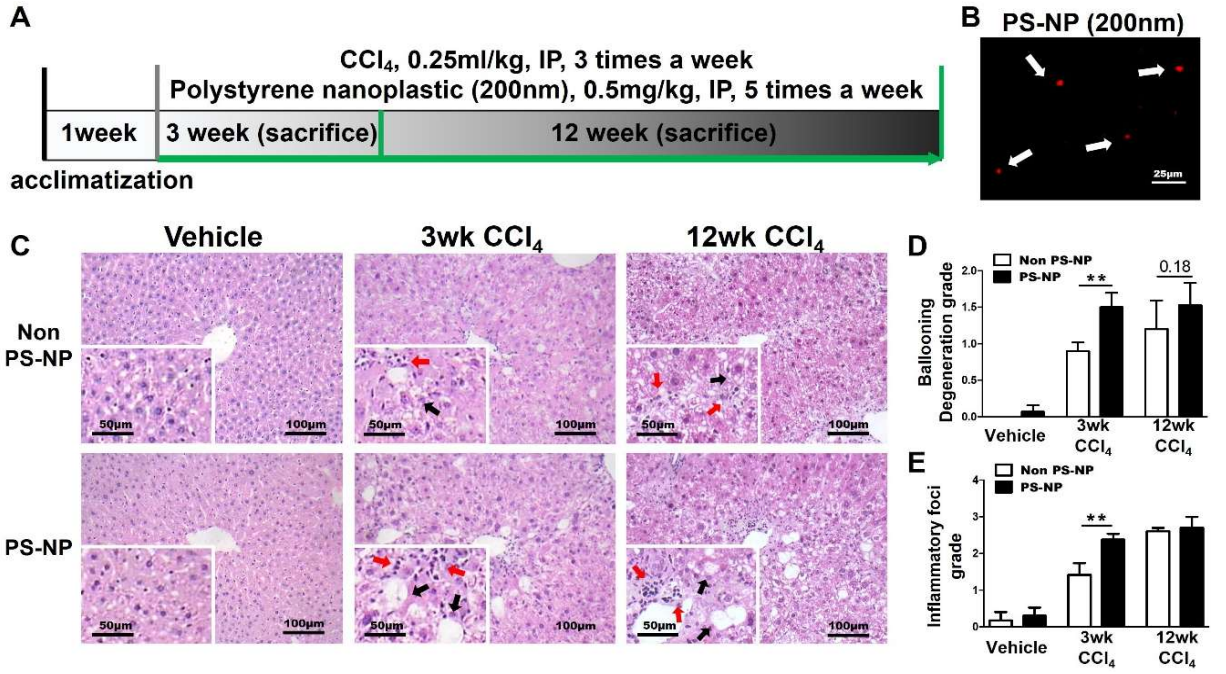

Fig. 1: Aggravation of CCl_4-induced liver damage by PS-NP administration. (A) Animal experiment design scheme used in this study. (B) Fluorescence images of PS-NP (arrows). (C) Representative photomicrograph of hematoxylin and eosin staining. The groups administered CCl_4 exhibited marked inflammation (red arrows) and ballooning degeneration (black arrows). (D) Histopathological grading of ballooning degeneration and (E) inflammatory foci. *P<0.05, **P<0.01, ***P<0.05.

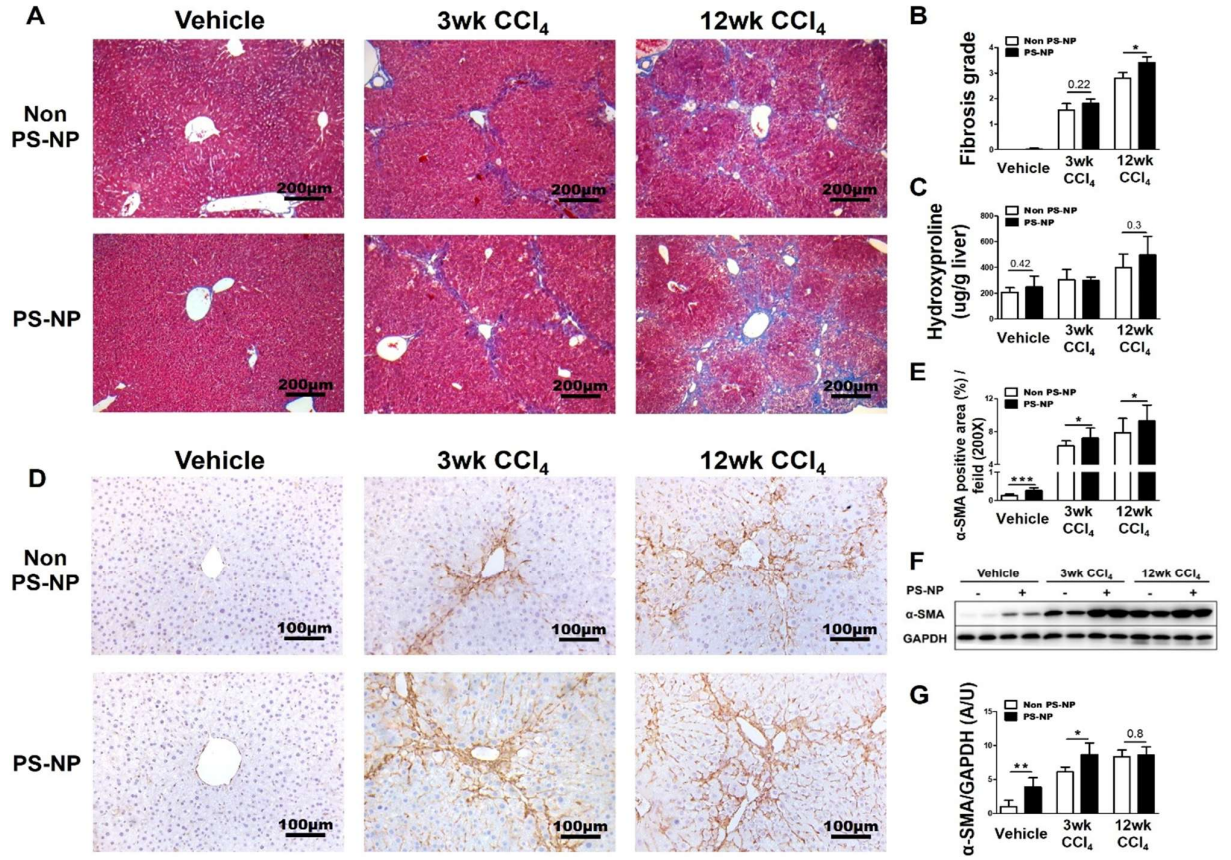

Fig. 2: Promotion of liver fibrosis and upregulation of α-SMA expression levels by PS-NP administration. (A) Representative photomicrograph of Masson's trichrome. (B) Histopathological grading of fibrosis. (C) Measurement of hepatic hydroxyproline. (D) Representative photomicrograph of immunohistochemistry of α-SMA. (E) Ratios of α-SMA-positive area in each group. (F) Immunoblotting for α-SMA. (G) Relative expression levels of α-SMA. The graph represents the relative band density compared with GAPDH. *P<0.05, **P<0.01, ***P<0.05.

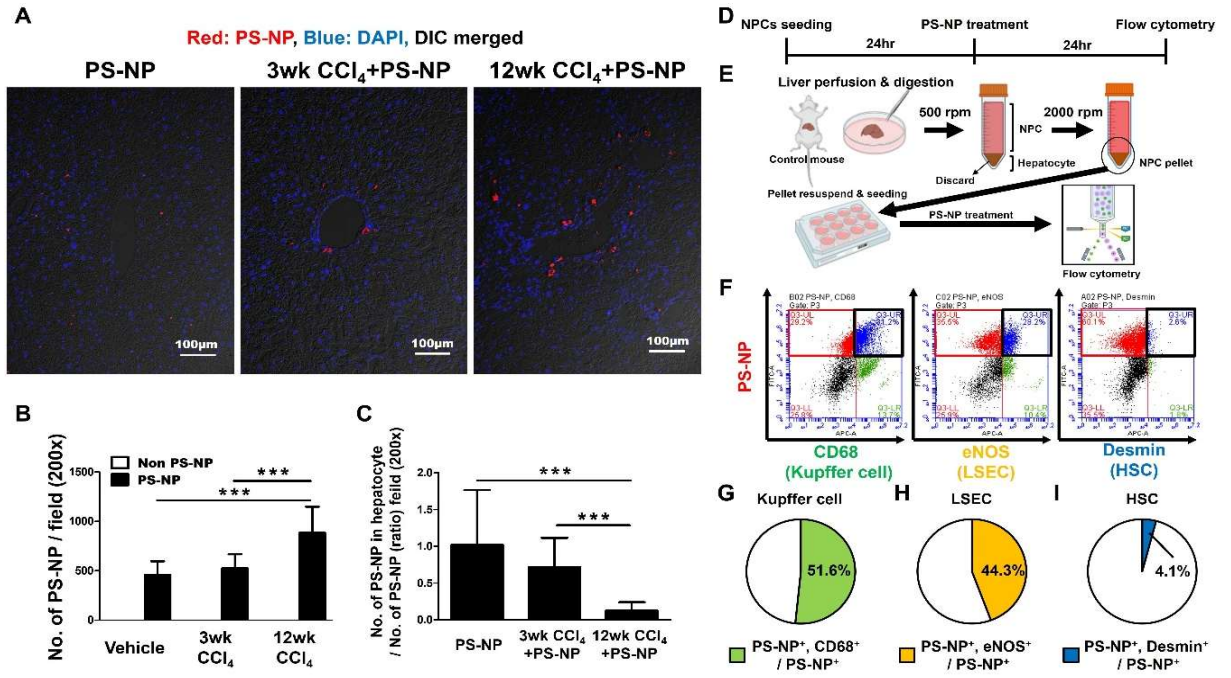

Fig. 3: Majority of PS-NPs accumulation and their distribution in the liver. (A) Representative photomicrograph of Immunofluorescence of PS-NPs (red) in liver tissue. (B) Number of PS-NPs for each group. (C) Ratio of PS-NP numbers in hepatocytes. (D, E) Experimental design for PS-NP treatment on NPC fractions. Created with BioRender.com. (F–I) Ratios of PS-NP-positive cells in each cell type. Flow cytometry analysis was performed in NPC fractions to determine the percentages of PS-NP-positive cells in each cell type, using CD68 for Kupffer cells, eNOS for LSECs, and desmin for HSCs. *P<0.05, **P<0.01, ***P<0.05.

PS-NPs were not associated with the release of TGF-β by CD68-positive cells: As the accumulation of PS-NPs induced more CD68-positive cell recruitment and *TGF-β* gene expression in the liver tissue, we then examined the effect of PS-NP-treated RAW 264.7 cells, which are CD68-positive, on LX-2 HSCs. (Fig. 5A). However, the supernatant from RAW 264.7 cells administered with PS-NPs did not upregulate α-SMA in LX-2 HSCs (Fig. 5B–D). Hence, although CD68-positive cells effectively engulfed PS-NPs, the expression of TGF-β was unrelated to the PS-NP treatment (Fig. 5E–G). Furthermore, TGF-β was not elevated by the supernatants from RAW 264.7 cells treated with PS-NPs (Fig. 5H). Moreover, IL-10 expression levels, which induce pro-fibrotic polarization of macrophages, did not increase significantly (Fig. 5I). PS-NPs only induced a significant up-regulation of TNF-α, pro-inflammatory cytokines, and weak increasing patterns of iNOS and IL-1β (Fig. 5J–L). These results indicate that PS-NPs promote the recruitment of CD68-positive cells but do not produce an effective stimulus for HSC activation.

PS-NPs became trapped in the α-SMA-positive region: To confirm the correlation between PS-NP and liver fibrosis, the number of accumulated PS-NPs and α-SMA expression levels were analyzed under fluorescence microscopy (Fig. 6A). Some of the PS-NPs were found between the α-SMA-positive area; this finding was more prevalent in the 12-week CCl_4+PS-NP group than the other groups. As the α-SMA-positive area increased, more PS-NPs were detected in the liver (Fig. 6B). In comparison to the PS-NP group, the quantity of PS-NPs significantly increased in the 12-week CCl_4+PS-NP group. Moreover, the 12-week CCl_4+PS-NP group exhibited a significantly larger merged area of PS-NPs and α-SMA than the PS-NP group and 3-week CCl_4+PS-NP group (Fig. 6C). These results indicate that PS-NPs accumulation was caused by the densely produced collagen bundles and promoted α-SMA expression.

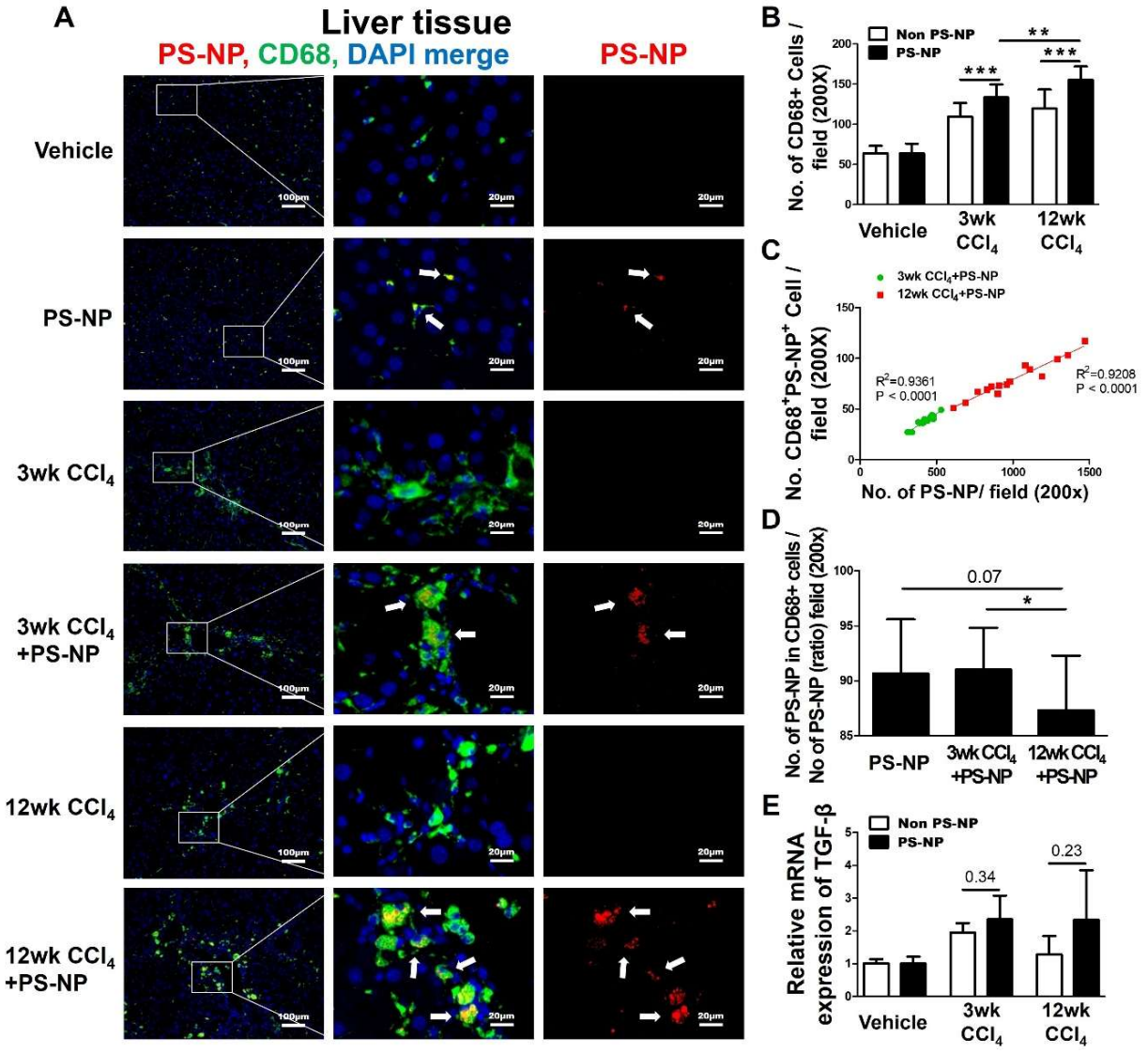

Fig. 4: Predominant engulfment of PS-NPs by CD68-positive cells. (A) Representative photomicrograph of immunofluorescence of PS-NPs (red) and CD68-positive Kupffer cells (green). Kupffer cells that retained NPs are shown in yellow in the merged images (arrows). (B) Number of CD68-positive cells for each group. (C) Correlation between the number of PS-NPs and the number of CD68-positive cells that engulfed PS-NPs. (D) Ratio of PS-NP numbers in CD68-positive cells for PS-NP administered groups. (E) RT-PCR analysis for TGF-β mRNA expression in liver. *P<0.05, **P<0.01, ***P<0.05.

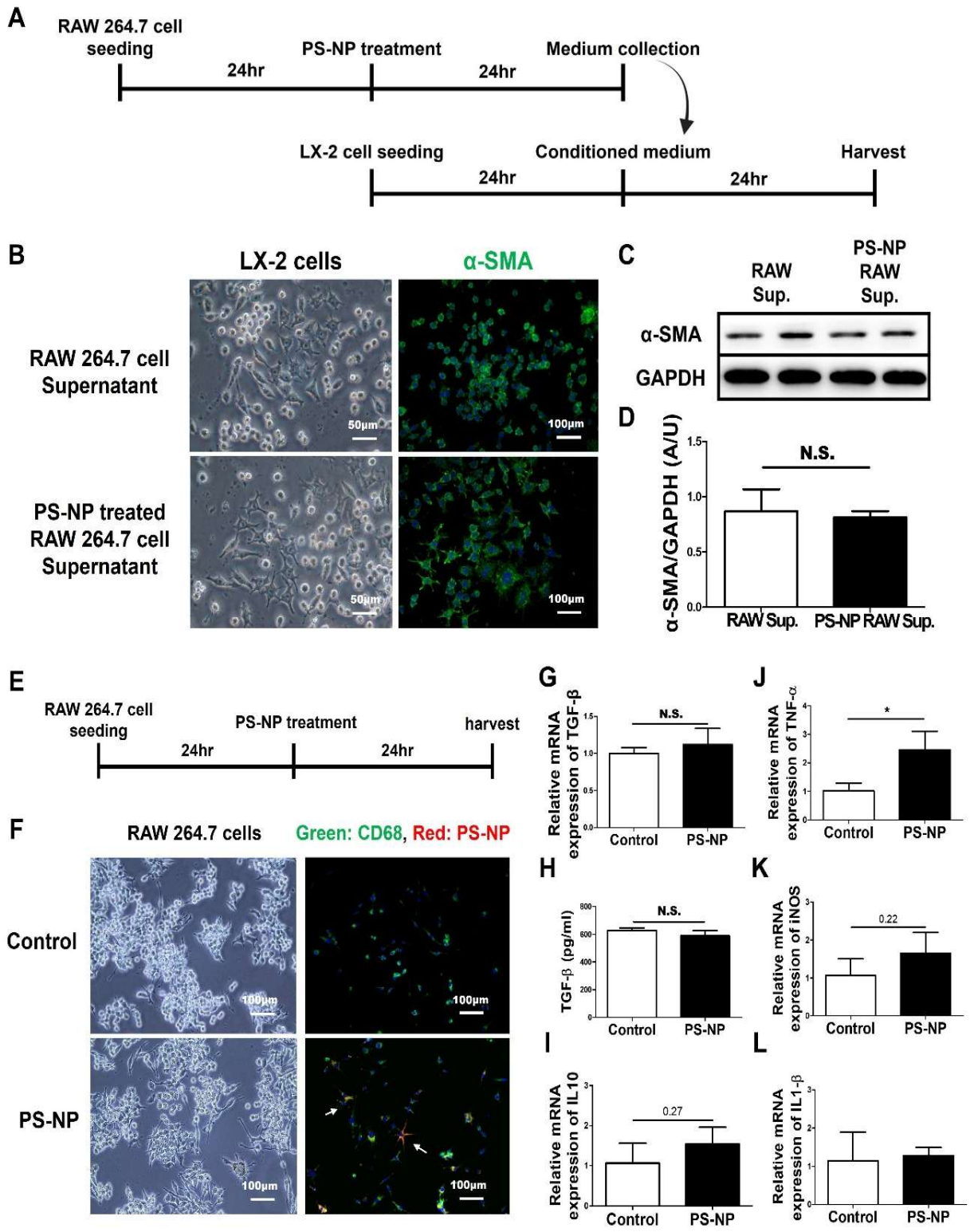

Fig. 5: Lack of association between PS-NPs and TGF-β secretion in CD68-positive cells. (A) Experimental design for RAW 264.7 cell supernatant treatment on LX-2 HSCs. (B) Representative photomicrograph of Immunofluorescence of α-SMA (green). (C) Immunoblotting for α-SMA. (D) Relative expression levels of α-SMA. The graph represents the relative band density compared with GAPDH. (E) Experimental design for PS-NP treatment on RAW 264.7 cells. (F) Representative photomicrograph of Immunofluorescence of CD68 (green) and PS-NPs (red). (G) RT-PCR analysis for *TGF-β* mRNA expression. (H) Quantification of TGF-β levels by ELISA. RT-PCR analysis for (I) *IL-10*, (J) *TNF-α*, (K) *iNOS*, (L) *IL-1β* mRNA expression. *P<0.05, **P<0.01, ***P<0.05.

PS-NPs directly promoted α-SMA expression in both LX-2 HSCs and primary isolated HSCs: Next, PS-NPs were treated to LX-2 HSCs to investigate whether PS-NPs directly promote HSC activation (Fig. 7A). Some PS-NPs were engulfed by LX-2 HSCs and were shown to merge with α-SMA in the IF staining analysis (Fig. 7B).

Additionally, LX-2 HSCs that engulfed PS-NPs showed higher α-SMA expression levels, which were mediated by phosphorylation of Smad2/3 (Fig. 7C–E). We further confirmed the increase in α-SMA expression levels in PS-NP-treated primary HSCs. To isolate primary HSCs, we used OptiPrep density gradient medium and treated the PS-NPs for 24h on the primary isolated HSCs (Fig. 7F, G). As shown in the LX-2 HSCs, treatment with PS-NPs induced nuclear translocation of Smad2/3 and significantly increased pSmad2/3 and α-SMA expression levels in primary HSCs (Fig. 7H–K). These results indicate that PS-NPs can be engulfed by HSCs and directly activate HSCs through the upregulation of the pSmad2/3 pathway.

PS-NPs promoted HSC activation by enhancing stretch-induced mechanical stress: To confirm whether PS-NPs promote the stimulation of TGF-β receptors, the expression levels of pTGFBR1 were analyzed (Fig. 8A). Higher expression of pTGFBR1 was confirmed in HSCs treated with PS-NPs (Fig. 8B, C). However, we could not confirm the co-localization between PS-NPs and pTGFBR1 in the confocal microscopy images (Fig. 8D). Notably, as the treatment time progressed, the pericellular PS-NPs were removed, revealing a space (yellow dotted line and arrows) between the PS-NPs and the HSCs (Fig. 8E). During this process, the HSCs extended cytoplasmic protrusions toward the PS-NPs, generating mechanical tension, which enhanced α-SMA expression.

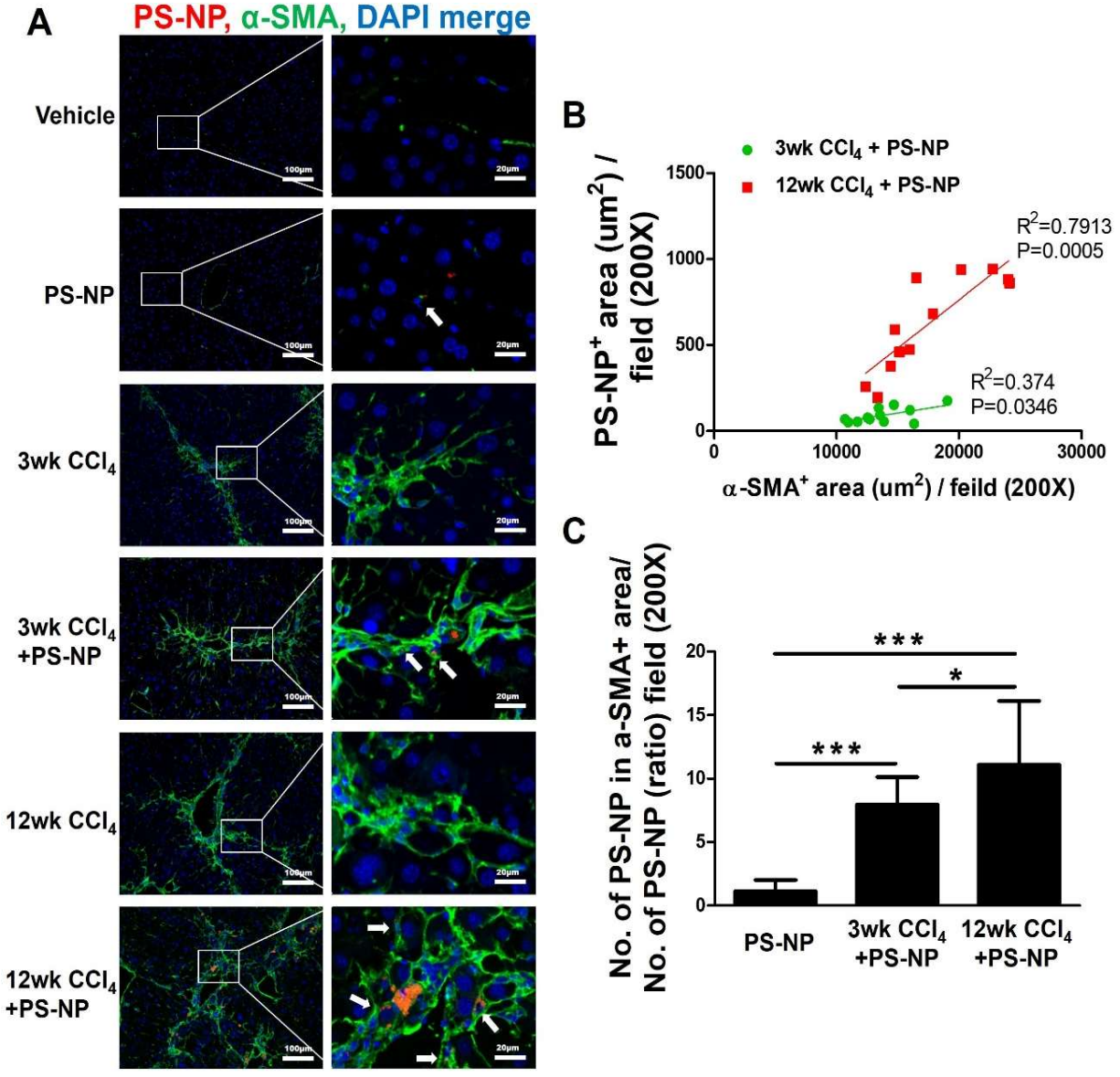

Fig. 6: Correlations between the number of PS-NPs and α-SMA-positive areas. (A) Representative photomicrograph of Immunofluorescence of PS-NPs (red) and a-SMA-positive HSCs and collagen bundles (green). Numerous PS-NPs were trapped in the α-SMA-positive area (arrows). (B) Correlation between the area of the α-SMA positive region and the area of PS-NPs. (C) Ratio of the number of PS-NPs in the α-SMA-positive area. *P<0.05, **P<0.01, ***P<0.05.

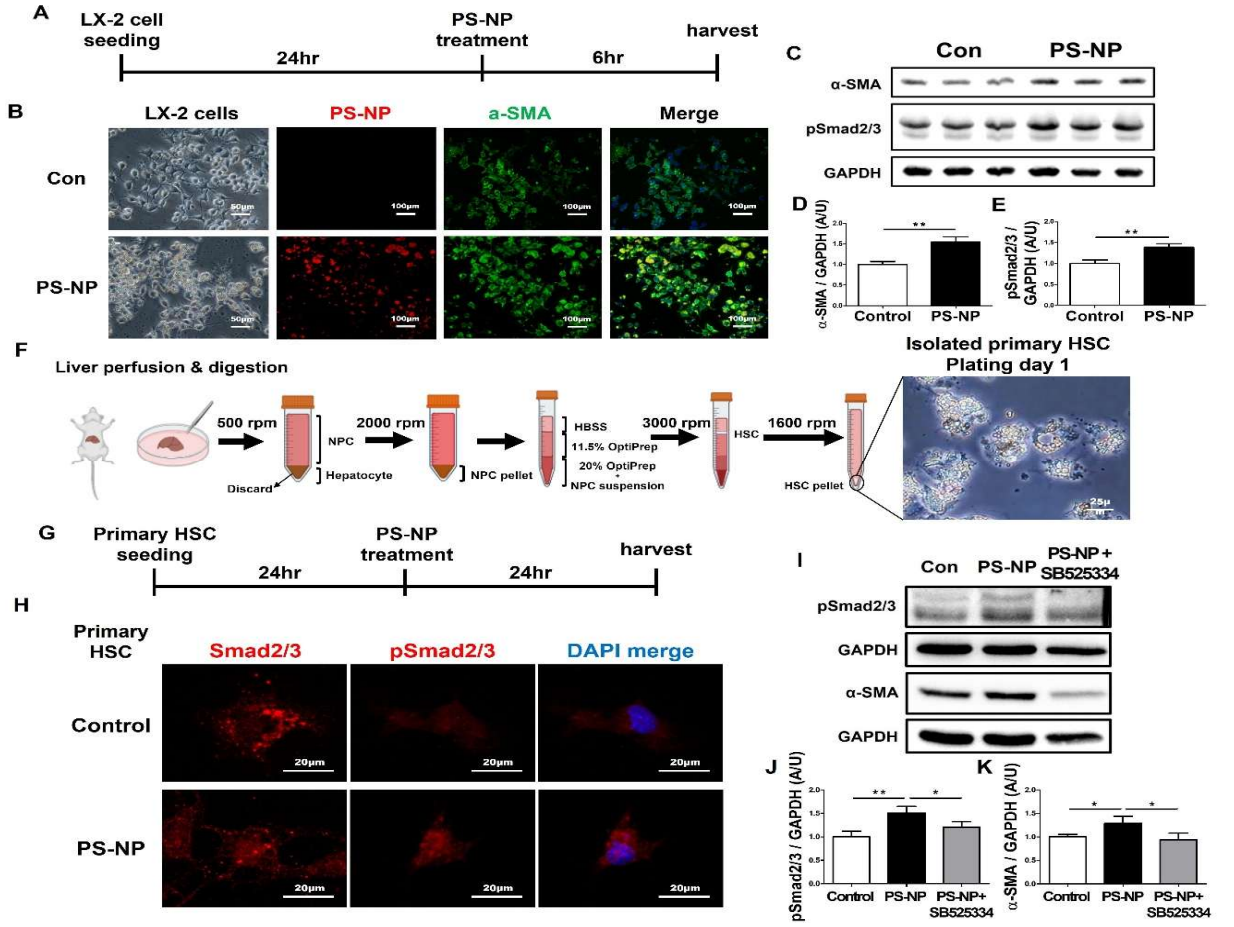

Fig. 7: Enhanced phospho-Smad2/3 and α-SMA expression by PS-NP treatments in LX-2 HSCs and primary HSCs. (A) Experimental design for PS-NP treatment on LX-2 HSCs. (B) Representative photomicrograph of Immunofluorescence of PS-NP (red) and α-SMA (green). (C) Immunoblotting for α-SMA and pSmad2/3. Relative expression levels of (D) α-SMA and (E) pSmad2/3. The graph represents the relative band density compared with GAPDH. (F) The procedure of mouse primary HSC isolation. Created with BioRender.com. (G) Experimental design for PS-NP treatment on HSCs. (H) Representative photomicrograph of Immunofluorescent of Smad2/3 (red) or pSmad2/3 (red). (I) Immunoblotting for pSmad2/3 and α-SMA. Relative expression levels of (J) pSmad2/3 and (K) α-SMA. The graph represents the relative band density compared to GAPDH. *P<0.05, **P<0.01, ***P<0.05.

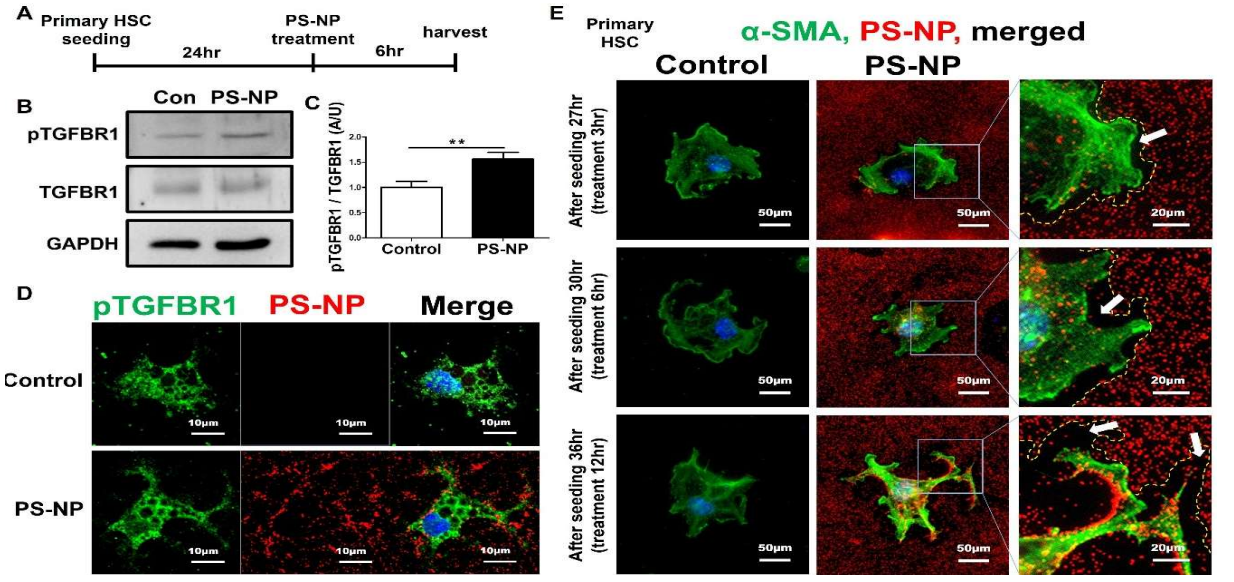

Fig. 8: Enhancement of stretch-induced mechanical stress of HSCs thereby PS-NPs promoting HSC activation. (A) Experimental design for PS-NP treatment on HSCs. (B) Immunoblotting for TGFBR1 and pTGFBR1. (C) Relative expression levels of pTGFBR1. The graph represents the relative band density compared to TGFBR1. (D) Representative confocal micrograph of pTGFBR1 (green) and PS-NP (red) in HSCs. (E) Time-dependent cytoplasmic changes in α-SMA-positive HSCs and PS-NPs (red) engulfment. A yellow dotted line and white arrows indicate the border of the space created by PS-NP engulfment. *P<0.05, **P<0.01, ***P<0.05.

DISCUSSION

This study demonstrates the PS-NPs exacerbate CCl_4-induced liver fibrosis and directly induce the activation of HSCs. Most PS-NPs or microplastics are ingested through drinking water and food, and only 1–4% translocate into the circulatory system after crossing the intestinal barrier (Hwang *et al.,* 2020). Meanwhile, the gut barrier must be destroyed to efficiently introduce PS-NPs into the liver through the intestine (Shi *et al.,* 2022). Therefore, we injected PS-NPs intraperitoneally to achieve effective hepatic accumulation, based on the maximum concentration of PS plastic particles detected in human blood (4.8μg/ml) (Leslie *et al.,* 2022). Subsequently, higher amounts of PS-NPs were observed to accumulate in liver fibrosis models compared to normal livers (Fig. 3B). PS-NPs were engulfed more by liver NPCs than by parenchymal cells, with the highest accumulation in KCs, followed by LSECs, and then HSCs (Fig. 3F–I). Since LSECs have special transcellular pores called fenestrae with diameters of 50–300 nm, it is thought that PS-NPs could sufficiently pass through fenestrae and reach HSCs and parenchymal cells (Czyzynska-Cichon *et al.,* 2024). Interestingly, progressive fibrosis was associated with reduced PS-NP uptake by KCs and increased accumulation in HSCs (Fig. 4D, 6C). This is attributed to PS-NPs becoming trapped within collagen fibers. Consequently, HSCs are persistently and directly stimulated by PS-NPs, leading to their activation.

In Fig. 2, the 12-week CCl_4+PS-NP group worsened collagen accumulation and fibrosis severity compared to 12-week CCl_4 group. However, quantification of the Western blot did not reveal any significant alterations in α-SMA expression between the 12-week CCl_4+PS-NP and 12-week CCl_4 groups. This discrepancy can be attributed to a biological ceiling effect in HSC activation. Interestingly, a previous study demonstrated that α-SMA expression levels reached their maximum at week 14 and declined at week 16 in a CCl_4-induced fibrosis model (Hong *et al.,* 2013). Additionally, C57BL/6 mice treated with CCl_4 for 12 and 16 weeks showed comparable severity of liver fibrosis (Madani *et al.,* 2025). Therefore, we suggest that HSCs had already reached their maximal activation capacity after 12 weeks of CCl_4 treatment; thus PS-NP seems not to affect a-SMA expression levels induced by CCl_4 at 12 weeks. Consequently, the higher fibrosis grade in the 12-week CCl_4+PS-NP group than in the 12-week CCl_4 was ultimately driven by the enhanced HSC activation by PS-NPs at week 3. While our findings suggest that HSC activation seems to reach its maximum level at 12 weeks of CCl_4 treatment, the lack of dose-dependent data limits the exact identification of the synergistic threshold. Therefore, future long-term studies with varying concentrations of CCl_4 and PS-NPs are necessary to fully unravel these complex interactions.

Many studies have reported that NPs trigger ROS production, damaging cellular macromolecules, including DNA, proteins, and lipids (Chen *et al.,* 2024; Mahmud *et al.,* 2024). Moreover, NPs can be categorized as "xenobiotic particles" as they are found in living organisms and can interact with the immune system (Joksimovic *et al.,* 2022; Khan and Jia, 2023). In this study, PS-NPs enhanced the severity of inflammatory foci grade and increased the number of CD68-positive cells (Fig. 1&4). Macrophages can be classified as pro-inflammatory M1 types, which are involved in host defense and cytokine production, or pro-fibrogenic M2 types, which contribute to tissue repair and fibrosis by secreting pro-fibrotic factors and promoting myofibroblast formation (Liu *et al.,* 2014). In the liver, pro-fibrogenic KCs promote the activation of HSCs by producing TGF-β, which then induces their differentiation into myofibroblasts and increases the expression of α-SMA (Dewidar *et al.,* 2019). In this study, KCs, which exhibited the highest PS-NP phagocytosis rate, were not involved in TGF-β regulation and were unrelated to α-SMA expression in HSCs (Fig. 5). These results confirmed that PS-NPs can induce pro-inflammatory stimuli that promote macrophage migration, but do not induce pro-fibrogenic differentiation in macrophages. Interestingly, PS-NPs directly increased pSmad2 (Ser465/467) and pSmad3(Ser423/425) expression levels in both LX-2 HSCs and primary isolated HSCs (Fig. 7). This indicates that Smad phosphorylation occurred at the C-terminal SSXS regions, which is triggered by TGF-β receptor 1 (Massague, 1998; Mori *et al.,* 2004). Therefore, these findings suggest that PS-NP-induced activation of HSCs was mediated through the TGF-β receptor.

This study assessed the spatial relationship between PS-NPs and pTGFBR1 (Fig. 8B&C). A prior study showed the phosphatidylserine receptor recognizes PS microparticles through its extracellular aromatic cluster (Kuroiwa *et al.,* 2023). Also, in human breast cancer cells, polystyrene-derived microplastics significantly stimulated non-genomic estrogen receptor and tumor growth in mice by stimulating the estrogen receptor (Lee *et al.,* 2025). These prior studies suggest the potential of PS-NPs as material stimulating receptors. This study did not identify any direct binding between the PS-NPs and pTGFBR1 (Fig. 8D).

We observed that HSCs actively attempted to engulf pericellular PS-NPs by stretching their cytoplasm. PS-NPs adhered to the cell membrane and were engulfed by HSCs (Fig. 8E). The phagocytic process requires actin cytoskeleton rearrangement, which induces membrane expansion with high tension, resulting in stretch-induced mechanical stress (Masters *et al.,* 2013; Cui *et al.,* 2014). Subsequently, increased cytoskeletal tension clusters integrins to initiate mechanotransduction (Nishimichi *et al.,* 2021). Especially, integrin αvβ3 regulates this phagocytosis and mediates HSC activation (Jiang *et al.,* 2012). Integrin-mediated activation of TGF-β induces autocrine signaling and increases phosphorylation of TGF-β receptor 1 (Sakata *et al.,* 2004; Sharip and Kunz, 2025). Collectively, these observations suggest that the mechanical stress generated by the stretching of cytoplasmic protrusions during PS-NP engulfment may contribute to HSC activation. Since the present study did not show direct biophysical measurements of HSC cellular tension, more additional research is needed to clarify the precise mechanisms for the activation of HSC by PS-NP. As xenobiotic particles, additional studies are needed to distinguish whether the mechanical stress on HSCs induced by PS-NPs arises from the chemical properties of polystyrene itself or from the physical characteristics associated with the 200nm particle size. Therefore, comprehensive research is essential to examine size- and

chemistry-dependent effects of nanoplastics specifically in liver cells and elucidate the mechanisms of intercellular communication triggered by cellular alterations induced by PS-NPs.

PS-NPs are engulfed by cells through multiple pathways, and their interactions with biomembranes are influenced by physicochemical properties such as surface charge and size (Bu *et al.,* 2024). In particular, clathrin-mediated endocytosis, caveolae-mediated endocytosis, and micropinocytosis may serve as major entry routes for PS-NPs (Monti *et al.,* 2015; Liu *et al.,* 2022). According to a study, 50nm PS-NPs enter cells through clathrin-mediated, caveolin-mediated, and macropinocytosis pathways. In contrast, larger PS-NPs utilize macropinocytosis or are unable to be internalized by cells (Liu *et al.,* 2021). HSCs, which are the most closely related to hepatocytes, can respond the quickest to hepatocyte destruction. HSCs exhibit sensitivity to apoptotic bodies and activate to manage this cellular debris (Zhan *et al.,* 2006). Given this, further investigation into the role of HSCs in the defense mechanisms of the hepatic sinusoidal wall is warranted and elucidating novel mechanisms of HSC function may provide a foundation for the development of innovative therapeutic strategies.

Conclusions: Since liver fibrosis could be induced by multiple cellular communication, the underlying mechanisms of HSC activation caused by nano- or microplastics require further investigation. Clarifying PS-NP effects on liver cells is expected to advance strategies for preventing and treating liver fibrosis. This research proposes that PS-NPs are xenobiotic particles that could directly promote HSC activation by stretch-induced mechanical stress, and chronic exposure to PS-NPs may induce more severe chronic liver diseases. Overall, to best of our knowledge, this study is the first to suggest that PS-NPs can exacerbate liver fibrosis and warns of the potential risks associated with chronic PS-NP exposure.

Authors contribution: JHY wrote the main manuscript text, performed visualization, and validation and contributed to the conceptualization and formal analysis of the study. JHY, TUK, WJK, HYK, SWL, and KKK conducted the investigation. JHY, MSS, SDK, YEC, SMB, SKC, and JKP provided substantial contributions to methodology. MSS, SDK, YEC, SMB, and SKC provided resources. JKP contributed to the conceptualization and formal analysis of the study and was involved in editing and supervision, writing-review and project administration.

Funding: This work was supported by National Research Foundation of Korea (NRF) grants funded by the Korea Government, the Ministry of Science and ICT (grant number RS-2024-0045-3894, RS-2024-00408854-0-2) and the 2025 Health Fellowship Foundation.

Data Availability: No data was used for the research described in the article.

Conflicts of Interest: The authors declare no conflict of interest.

Acknowledgements: Not applicable

REFERENCES

Baek SM, Kim TU, Lee YJ, *et al.,* 2023. Disrupted intestinal mucosal barrier mediated by alcohol consumption aggravates systemic microplastic accumulation. Ecotoxicology and Environmental Safety 262:115342.

Barnes DK, Galgani F, Thompson RC, *et al.,* 2009. Accumulation and fragmentation of plastic debris in global environments. Philosophical Transactions of the Royal Society B: Biological Sciences 364(1526):1985-98.

Bu W, Cui Y, Jin Y, *et al.,* 2024. Unmasking the invisible threat: Biological impacts and mechanisms of polystyrene nanoplastics on cells. Toxics 12(12).908.

Chen X, Xuan Y, Chen Y, *et al.,* 2024. Polystyrene nanoplastics induce intestinal and hepatic inflammation through activation of nf-kappab/nlrp3 pathways and related gut-liver axis in mice. Science of the Total Environment 935:173458.

Chen Y, Jin H, Xue Y, *et al.,* 2025. Evaluating the hepatotoxicity of polyvinyl chloride microplastics in ducks: oxidative and fibrotic outcomes. Pakistan Veterinary Journal 45(4):1733-43.

Cheng Z, Fu L, Yimamu M, *et al.,* 2025. Fenofibrate Inhibits Hepatic Stellate Cell Activation and Autophagy in Liver Fibrosis through the Tgfβ1/Smad3 and Pparα/Cgas/Sting Pathways. Pakistan Veterinary Journal 45(2):579-91.

Cui X, Zhang X, Yin Q, *et al.,* 2014. F actin cytoskeleton reorganization is associated with hepatic stellate cell activation. Molecular Medicine Reports 9:1641-47.

Czyzynska-Cichon I, Kotlinowski J, Blacharczyk O, *et al.,* 2024. Early and late phases of liver sinusoidal endothelial cell (lsec) defenestration in mouse model of systemic inflammation. Cellular & Molecular Biology Letters 29(1):139.

Deng Y, Zhang Y, Lemos B, *et al.,* 2017. Tissue accumulation of microplastics in mice and biomarker responses suggest widespread health risks of exposure. Scientific Reports 7:46687.

Dewidar B, Meyer C, Dooley S, *et al.,* 2019. TGF-beta in hepatic stellate cell activation and liver fibrogenesis-updated 2019. Cells 8(11).1419.

Ding H, Chen J, Qin J, *et al.,* 2021. TGF-beta-induced alpha-SMA expression is mediated by c/EBPBETA acetylation in human alveolar epithelial cells. Molecular Medicine 27(1):22. https://doi.org/10.1186/s10020-021-00283-6

Faria SC, Ganesan K, Mwangi I, *et al.,* 2009. MR imaging of liver fibrosis: Current state of the art. Radiographics 29(6):1615-36.

Gupta C, Kaushik S, Himanshu, *et al.,* 2022. Bioaccumulation and toxicity of polystyrene nanoplastics on marine and terrestrial organisms with possible remediation strategies: A review. Environmental Advances 8. 100227. https://doi.org/10.1016/j.envadv.2022.100227

Gupta P, Sata TN, Yadav AK, *et al.,* 2019. TGF-beta induces liver fibrosis via mirna-181a-mediated down regulation of augmenter of liver regeneration in hepatic stellate cells. PLoS One 14(6):e0214534.

Hale RC, Seeley ME, La Guardia MJ, *et al.,* 2020. A global perspective on microplastics. Journal of Geophysical Research: Oceans 125(1). https://doi.org/10.1029/2018JC014719

Hong IH, Park SJ, Goo MJ, *et al.,* 2013. JNK1 and JNK2 regulate α-SMA in hepatic stellate cells during CCl4 -induced fibrosis in the rat liver. Pathology International 63(10):483-91.

Hu M and Palic D, 2020. Micro- and nano-plastics activation of oxidative and inflammatory adverse outcome pathways. Redox Biology 37:101620. https://doi.org/10.1016/j.redox.2020.101620

Hwang J, Choi D, Han S, *et al.,* 2020. Potential toxicity of polystyrene microplastic particles. Scientific Reports 10(1):7391.

Joksimovic N, Selakovic D, Jovicic N, *et al.,* 2022. Nanoplastics as an invisible threat to humans and the environment. Journal of Nanomaterials 2022: 6707819 https://doi.org/10.1155/2022/6707819

Jiang JX, Chen X, Hsu DK, *et al.,* 2012. Galectin-3 modulates phagocytosis-induced stellate cell activation and liver fibrosis in vivo. American Journal of Physiology-Gastrointestinal and Liver Physiology 302(4):G439-46.

Jung YR, Yim JH, Lee YJ, *et al.,* 2024. Decreased SMP30 Expression Is Related with EMT in the Kidneys of Two Siberian Tigers With CKD. In Vivo 38(1):226-34.

Khan A and Jia Z, 2023. Recent insights into uptake, toxicity, and molecular targets of microplastics and nanoplastics relevant to human health impacts. iScience 26(2):106061.

Kim TU, Park JS, Yim JH, *et al.,* 2025. Uterine angiomyofibroblastoma in a domestic cat: A need of precise diagnosis for proper perioperative management. Veterinární Medicína 70(5):177-83.

Kleiner DE, Brunt EM, Van Natta M, *et al.,* 2005. Design and validation of a histological scoring system for nonalcoholic fatty liver disease. Hepatology 41(6):1313-21.

Kuroiwa M, Yamaguchi SI, Kato Y, *et al.,* 2023. Tim4, a macrophage receptor for apoptotic cells, binds polystyrene microplastics via aromatic-aromatic interactions. Science of the Total Environment 875:162586.

Kwon W, Kim D, Kim HY, *et al.,* 2022. Microglial phagocytosis of polystyrene microplastics results in immune alteration and apoptosis in vitro and in vivo. Science of the Total Environment 807(Pt 2):150817.

Lee SW, Kim HY, Jang S, *et al.,* 2025. Exploratory investigation of the correlation between microplastics and breast cancer: Polystyrene-derived microplastics promote cell proliferation via estrogenic endocrine disruption. Journal of Environmental Chemical Engineering 13(2):115473. https://doi.org/10.1016/j.jece.2025.115473.

Lee WS, Cho HJ, Kim E, *et al.,* 2019. Bioaccumulation of polystyrene nanoplastics and their effect on the toxicity of au ions in zebrafish embryos. Nanoscale 11(7):3396.

Leslie HA, van Velzen MJM, Brandsma SH, *et al.,* 2022. Discovery and quantification of plastic particle pollution in human blood. Environment International 163:107199.

Lin Y, Fang ZP, Liu HJ, *et al.,* 2017. HGF/R-spondin1 rescues liver dysfunction through the induction of $Lgr5^+$ liver stem cells. Nature Communications 8(1):1175.

Lin Z, Monteiro-Riviere NA and Riviere JE, 2015. Pharmacokinetics of metallic nanoparticles. Wiley Interdisciplinary Reviews: Nanomedicine and Nanobiotechnology 7(2):189-217.

Liu L, Xu K, Zhang B, *et al.,* 2021. Cellular internalization and release of polystyrene microplastics and nanoplastics. Science of the Total Environment 779:146523.

Liu YC, Zou XB, Chai YF, *et al.,* 2014. Macrophage polarization in inflammatory diseases. International Journal of Biology Sciences 10(5):520-29.

Liu YY, Liu J, Wu H, *et al.,* 2022. Endocytosis, distribution, and exocytosis of polystyrene nanoparticles in human lung cells. Nanomaterials (Basel) 13(1):84. https://doi.org/10.3390/nano13010084.

Madani J, Li J, Ching MEA, *et al.,* 2025. CD8 T Cell Hyperfunction and Reduced Tumour Control in Murine Models of Advanced Liver Disease. European Journal of Immunology 55(8):e70026.

Mahmud F, Sarker DB, Jocelyn JA, *et al.,* 2024. Molecular and cellular effects of microplastics and nanoplastics: Focus on inflammation and senescence. Cells 13(21):1788. https://doi.org/10.3390/cells13211788.

Massague J, 1998. Tgf-beta signal transduction. Annual Review of Biochemistry 67:753-91.

Masters TA, Pontes B, Viasnoff V, *et al.,* 2013. Plasma membrane tension orchestrates membrane trafficking, cytoskeletal remodeling, and biochemical signaling during phagocytosis. Proceedings of the National Academy of Sciences 110(29):11875-80.

Monti DM, Guarnieri D, Napolitano G, *et al.,* 2015. Biocompatibility, uptake and endocytosis pathways of polystyrene nanoparticles in primary human renal epithelial cells. Journal of Biotechnology 193:3-10.

Mori S, Matsuzaki K, Yoshida K, *et al.,* 2004. Tgf-beta and hgf transmit the signals through jnk-dependent smad2/3 phosphorylation at the linker regions. Oncogene 23(44):7416-29.

Nishimichi N, Tsujino K, Kanno K, *et al.,* 2021. Induced hepatic stellate cell integrin, α8β1, enhances cellular contractility and TGFβ activity in liver fibrosis. The Journal of Pathology 253(4):366-73.

Nor NHM, Kooi M, Diepens NJ, *et al.,* 2021. Lifetime accumulation of microplastic in children and adults. Environmental Science & Technology 55(8):5084-96.

Oliveri Conti G, Ferrante M, Banni M, *et al.,* 2020. Micro- and nano-plastics in edible fruit and vegetables. The first diet risks assessment for the general population. Environmental Research 187:109677.

Park O, Jeong WI, Wang L, *et al.,* 2009. Diverse roles of invariant natural killer T cells in liver injury and fibrosis induced by carbon tetrachloride. Hepatology 49(5):1683-94.

Poitout-Belissent F, Aulbach A, Tripathi N, *et al.,* 2016. Reducing blood volume requirements for clinical pathology testing in toxicologic studies-points to consider. Veterinary Clinical Pathology 45:534-51.

Sakata R, Ueno T, Nakamura T, *et al.,* 2004. Mechanical stretch induces tgf-β synthesis in hepatic stellate cells. European Journal of Clinical Investigation 34(2):129-36.

Savoca MS, Wohlfeil ME, Ebeler SE, *et al.,* 2016. Marine plastic debris emits a keystone infochemical for olfactory foraging seabirds. Science Advances 2(11):e1600395.

Sharip A and Kunz, 2025. Mechanosignaling via Integrins: Pivotal Players in Liver Fibrosis Progression and Therapy. Cells 14(4):266.

Sharma VK, Ma XM, Lichtfouse E, *et al.,* 2023. Nanoplastics are potentially more dangerous than microplastics. Environmental Chemistry Letters 21(4):1933-36.

Shi C, Han X, Guo W, *et al.,* 2022. Disturbed gut-liver axis indicating oral exposure to polystyrene microplastic potentially increases the risk of insulin resistance. Environment International 164:107273.

Şimsek I, Arslan Yuce P, Gul G, *et al.,* 2025. Evaluation of toxic effects of silver micro and nanoparticles and silver nitrate in crayfish (Astacus leptodactylus). Pakistan Veterinary Journal 45(3):1389-95.

Sun J, Wu Y, Long C, *et al.,* 2018. Anthocyanins isolated from blueberry ameliorates CCl_4 induced liver fibrosis by modulation of oxidative stress, inflammation and stellate cell activation in mice. Food and Chemical Toxicology 120:491-99.

Tashiro K, Satoh A, Utsumi T, *et al.,* 2013. Absence of nogo-b (reticulon 4b) facilitates hepatic stellate cell apoptosis and diminishes hepatic fibrosis in mice. The American Journal of Pathology 182(3):786-95.

Tsuchida T, Friedman SL, 2017. Mechanisms of hepatic stellate cell activation. Nature Reviews Gastroenterology & Hepatology 14(7):397-411.

Wells RG, 2005. The role of matrix stiffness in hepatic stellate cell activation and liver fibrosis. Journal of Clinical Gastroenterology 39(4 Suppl 2):S158-161.

Xu J, Sui J, Luo Y, *et al.,* 2025. The protective and therapeutic effects of herbal medicines on hepatic disorders in animals. Pakistan Veterinary Journal 45(4):1491-502.

Xu Y, Peng Z, Ji W, *et al.,* 2015. A novel matrine derivative wm130 inhibits activation of hepatic stellate cells and attenuates dimethylnitrosamine-induced liver fibrosis in rats. BioMed Research International 2015:203978.

Yanguas SC, Cogliati B, Willebrords J, *et al.,* 2016. Experimental models of liver fibrosis. Archives of Toxicology 90(5):1025-48.

Yasin NAE, El-Naggar ME and Ahmed ZSO, *et al.,* 2022. Exposure to polystyrene nanoparticles induces liver damage in rat via induction of oxidative stress and hepatocyte apoptosis. Environmental Toxicology and Pharmacology 94:103911.

Yi SH, Zhang Y, Tang D, *et al.,* 2015. Mechanical force and tensile strain activated hepatic stellate cells and inhibited retinol metabolism. Biotechnology Letters 37(6):1141-52.

Zhan SS, Jiang JX and Wu J, *et al.,* 2006. Phagocytosis of apoptotic bodies by hepatic stellate cells induces nadph oxidase and is associated with liver fibrosis in vivo. Hepatology 43(3):435-43.